PERIODICO di MINERALOGIA
established in 1930

Dipartimento
di Scienze della Terra

Sapienza
Università di Roma

An International Journal of
Mineralogy, Crystallography, Geochemistry,
Ore Deposits, Petrology, Volcanology
and applied topics on Environment, Archaeometry and Cultural Heritage

U-Pb zircon and Ar-Ar amphibole ages from Sardinian migmatites (Italy) and review of migmatite ages from the Variscan belt

Gabriele Cruciani [1], Marcello Franceschelli [1,*], Antonio Langone [2], Mariano Puxeddu [3]

[1] Department of Chemical and Geological Sciences, Università di Cagliari, S.S. 554 Cittadella Universitaria, Monserrato (CA), 09042, Italy
[2] Institute of Geosciences and Georesources CNR, UOS of Pavia, via Ferrata 1, 27100 Pavia, Italy
[3] Formerly attached to Institute of Geosciences and Georesources CNR, via Moruzzi 1, 56124 Pisa, Italy

ARTICLE INFO

Submitted: January 2019
Accepted: March 2019
Available on line: April 2019

* Corresponding author:
francmar@unica.it

DOI: 10.2451/2019PM850

How to cite this article:
Cruciani G. et al. (2019)
Period. Mineral. 88, 203-209

ABSTRACT

U-Pb zircon age determinations and Ar-Ar dating on biotite and amphibole were performed on amphibole-bearing migmatite of NE Sardinia Variscan chain. The mesosome zircons yielded a weighted average age of 461.3 ± 3.3 Ma (U-Pb concordant data). Leucosome yielded U-Pb zircon ages clustering around 460 Ma (weighted average age of 462.5 ± 2.4 Ma, U-Pb concordant data) in core and oscillatory zoning domains. Zircon rims yielded an average value of 324.2 ± 4.0 Ma. The Ar-Ar amphibole age of 317.4 ± 2 Ma is interpreted as the age of chemical re-equilibration and cooling of this mineral. An Ar-Ar age determination on biotite yielded a total gas age of 283 Ma interpreted as a minimum argon age owing to Ar loss due to interlayered chlorite. The migmatite age of 324.2 ± 4.0 Ma fall in the 335-320 Ma interval that concentrates 76% of migmatite ages from the Variscan Belt.

Keywords: Migmatite; U-Pb zircon geochronology; Ar-Ar dating; Middle-Ordovician protolith; Variscan Sardinia.

INTRODUCTION

The Variscan metamorphic basement of northern Sardinia is mainly composed by igneous- and sedimentary-derived migmatite**s** (Cruciani et al., 2014a,b; Fancello et al., 2018). The age of migmatization in Sardinia is still poorly constrained. The first attempt to date the migmatization event in northeastern Sardinia was by Ferrara et al. (1978) who analysed by the Rb/Sr method a banded migmatite interpreted to have been derived from metamorphic differentiation. Six bands of this migmatite, treated as a whole-rock sample, fitted a Rb/Sr isochron of 344±7 Ma. These authors suggested that at this time, which corresponds to the metamorphic climax, the banded migmatite became a closed system. In the Migmatite Complex, Cruciani et al. (2008) described an amphibole-bearing migmatite cropping out along the north-eastern coast of Sardinia which was derived from a mid-Ordovician granitoid (biotite+plagioclase+quartz-bearing protolith) that underwent migmatization during the Variscan orogeny. Partial melting P-T conditions, estimated by P-T pseudosection approach, are 700-750 °C and ~13 kbar (Massonne et al., 2013). These authors also estimated P-T conditions of about 10.5 kbar and 700 °C for the crystallization of amphibole in the leucosome melt, and 9 kbar and 680 °C for the complete crystallization of this melt.

In this paper a geochronological study was performed on the leucosome and mesosome portions of a selected amphibole-bearing migmatite sample by means of U-Pb zircon dating and Ar-Ar on amphibole and biotite geochronology. The radiometric data obtained are discussed in the context of the metamorphic evolution of the Variscan belt in Sardinia and compared with radiometric data of migmatites from other European Variscan terranes. The aims of the paper are: (i) to increase the geochronological dataset referring to the migmatization event in Variscan Sardinia and (ii) to shed some light on the widespread migmatization event occurred during the Variscan cycle.

GEOLOGICAL SETTING AND FIELD OCCURRENCE

The Sardinian metamorphic basement belongs to the southern European Variscan belt. This basement, which underwent polyphase tectono-metamorphic evolution, is divided into three main tectono-metamorphic zones (Figure 1a): the External Zone in southwestern Sardinia, the Nappe Zone, including the External and Internal Nappe Zones, in the central part of the island, and the

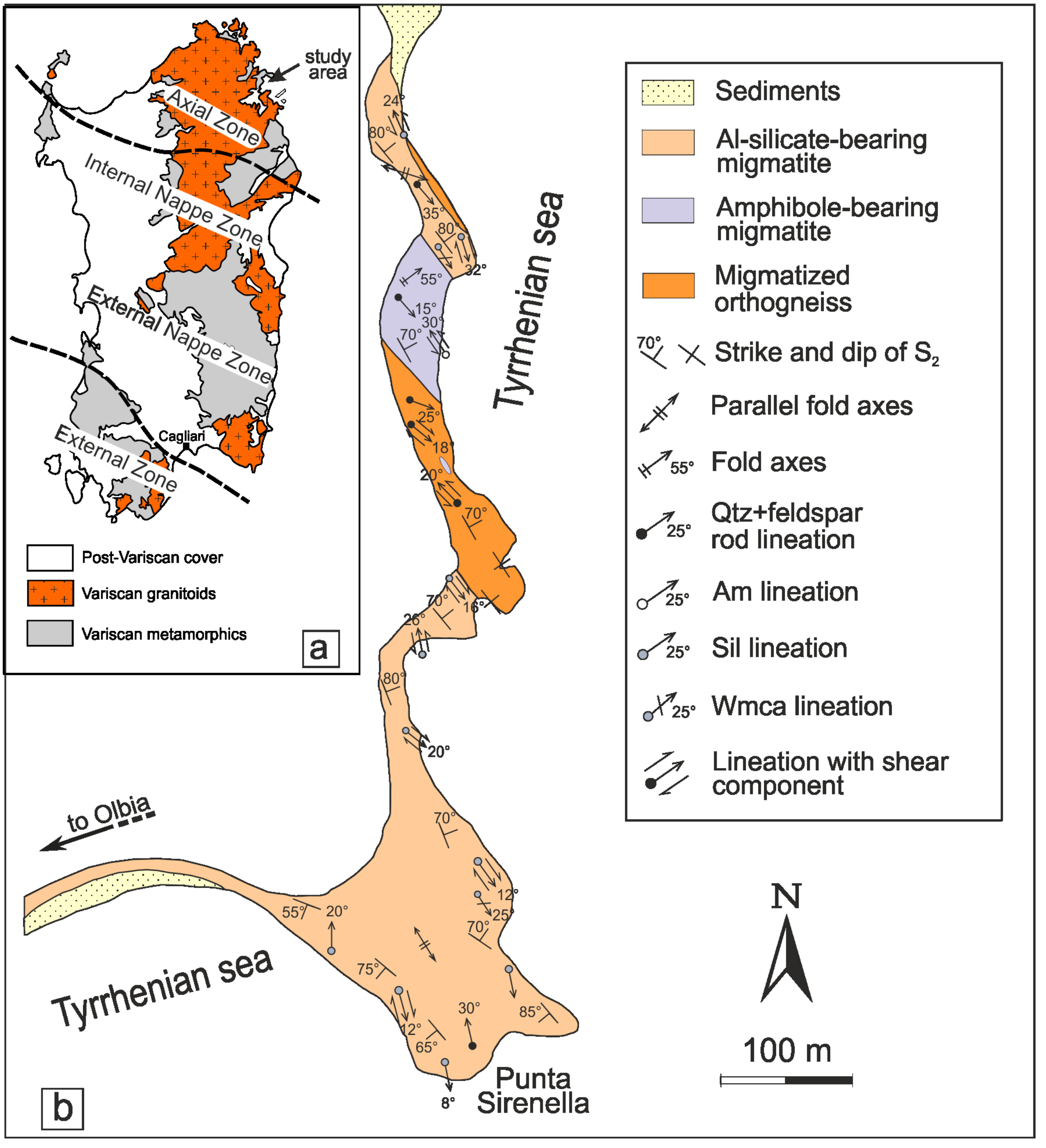

Figure 1. (a) Tectono-metamorphic zones of the Variscan chain of Sardinia (modified after Carmignani et al., 2001); (b) Geological sketch map of the migmatite outcrop of Punta Sirenella, northeastern Sardinia (modified after Cruciani et al., 2008). Abbreviations: Qtz: quartz; Am: amphibole; Sil: sillimanite; Wmca: white mica.

Axial Zone in northeastern Sardinia (Carmignani et al., 2001, and references therein). The Axial Zone also extends to southern Corsica (Rossi et al., 2009; Massonne et al., 2018). The metamorphic grade increases from sub-greenschist facies in the External Zone (Cruciani et al., 2016; Franceschelli et al., 2017) to amphibolite facies in the Axial Zone (Franceschelli et al., 1982; 1990; Connolly et al., 1994). The Axial Zone includes the Low to Medium Grade Metamorphic Complex (L-MGMC), mostly showing amphibolite facies assemblages, and the High Grade Metamorphic Complex (HGMC) or Migmatite Complex, whose metamorphism attains the sillimanite + K-feldspar isograd in the migmatites with both igneous and sedimentary protoliths (Cruciani et al., 2001). These two complexes are separated by the Posada-Asinara Line (PAL), a regional scale tectonic line interpreted as a major Variscan shear zone (Helbing and Tiepolo, 2005; Padovano et al., 2012). The migmatites also include hectometric metabasite lenses with eclogite (Cruciani et al., 2010, 2011, 2015a; Franceschelli et al., 2005a) and granulite facies relics and calc-silicate rocks.

Ordovician acidic calcalkaline products are distributed within the tectonic units from the foreland to the inner zone of the chain (Oggiano et al., 2010; Gaggero et al., 2012; Columbu et al., 2015; Musumeci et al., 2015). Variscan metamorphics are intruded by granitoids of the Corsica-Sardinia batholith (Casini et al., 2012, 2014, 2015 and references therein) and are unconformably covered by Late Carboniferous-Early Permian sedimentary deposits (Barca et al., 1995). An overall description of the Variscan metamorphism and deformations can be found in Franceschelli et al. (2005b), Rossi et al. (2009) and Cruciani et al. (2015b).

Amphibole bearing- migmatite: field occurrence

The studied sample belongs to the Migmatite Complex, a few kilometers northeast of Olbia, along the coast between Punta Sirenella and Punta Bados (Figure 1b). The amphibole-bearing migmatites (Figure 2 a,b) outcrop as a 100 m-long, 50-70 m large lens-shaped body, located between migmatized orthogneisses to the south and Al-silicate-bearing migmatites to the north (Figure 1). These amphibole-bearing migmatites are featured by the presence of millimeter to centimeter-sized euhedral amphibole crystals in leucosomes (Figure 2b) and by a discontinuous alternation of tonalitic and granodioritic leucosomes and mesosomes. The amphibole-bearing migmatites are characterized by the presence of a pervasive foliation (S_2), with a N145° strike and 80° dip, transposing leucosomes and quartz-feldspatic "rods" in the XY plane (Cruciani et al., 2008). The evidence of a previous deformation is given by the presence of a gneiss-like layering (D_1) predating the most pervasive folding phase D_2. In the XY plane an oriented biotite lineation with a N139 strike and a SE 15° dip is recognizable. Decimeter-sized sheath folds parallel to the biotite lineation were also observed.

SUMMARY OF LEUCOSOME AND MESOSOME PETROGRAPHY

The petrographic features of the amphibole-bearing migmatites from Punta Sirenella were described by Cruciani et al. (2008, 2014a) and by Massonne et al. (2013) to which the reader is referred for a detailed petrographic description. Two samples (mesosome MES5 and leucosome LEU5) were selected for geochronological investigation. Sample LEU5 (Figure 2c) is made up of plagioclase (45 vol%), quartz (35 vol%), K-feldspar (<2 vol%), amphibole (10 vol%), biotite (7 vol%) and garnet (1 vol%) whereas sample MES5 (Figure 2d) consists of plagioclase (40 vol%), quartz (32 vol%), K-feldspar (<2 vol%), amphibole (5 vol%), biotite (20 vol%) and garnet (1 vol%). Accessory apatite, zircon, titanite, Fe-oxides, epidote and monazite were found in both samples. Amphibole is surrounded by a matrix of quartz, plagioclase and subordinate biotite. Amphibole of the leucosome contains several rounded inclusions of plagioclase, quartz and subordinate garnet. Garnet inclusions in amphibole occur as very small fractured and corroded grains surrounded by thin coronas of plagioclase. In the quartzo-feldspathic matrix of the mesosome sample, biotite marks the foliation.

MINERAL CHEMISTRY

Selected trace elements and Rare Earth Element (REE) abundances in zircons, distinguished between core and rim, of several zircon grains from leucosome sample LEU5 are given in Table 1.

On the basis of cathodoluminescence (CL) imaging (Figure 3) three zircon populations can be distinguished in the leucosomes and mesosomes of the amphibole-bearing migmatites of Punta Sirenella. They are, in order of increasing abundance: (i) elongated prismatic crystals up to a maximum of 250-300 μm long characterized by concentric, oscillatory zoning typical of magmatic growth (Figures 3 a,b); (ii) elongated to rounded-shaped zircons, between 100 and 150 μm in size, with relics of darker inner cores overgrown and/or truncated by bright external rims of some dozens microns in thickness (Figures 3 c,d). Sometimes concentric zoning is preserved in the core and sporadically bright domains are also observed in the inner portions of these zircons; (iii) 50 μm-sized anhedral to rounded zircon grains, with a very slight non-concentric zonation (not shown in Figure 3). All zircons display fractionated chondrite-normalized REE patterns with HREE enrichment, positive anomalies for Ce and negative anomalies for Eu (Figure 4). ΣREE in zircon core is higher (364-759 ppm) as compared to rim

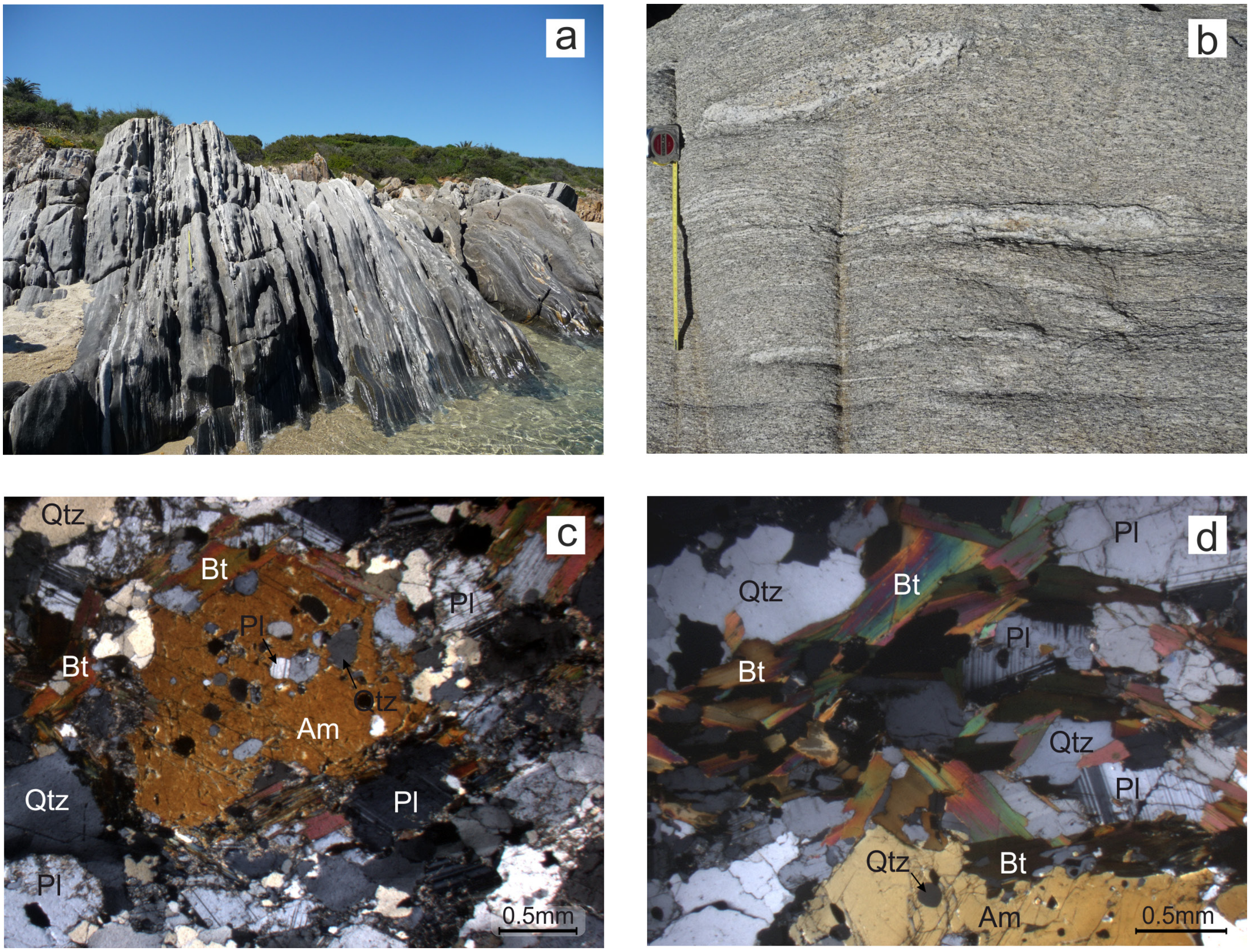

Figure 2. Field photographs (a,b) and photomicrographs (c,d) of the amphibole-bearing migmatites of NE Sardinia. (a) Layered aspect of the amphibole-bearing migmatites; at the right hand side of the picture, the brownish rocks on the background are Al-silicate bearing migmatites in contact with the amphibole-bearing migmatites. (b) leucosome with amphibole crystals visible by the naked eye (upper left corner of the picture) and folded, amphibole-bearing leucosomes in the migmatite (lower part of the picture); the greysh, foliated rock hosting the leucosome is mesosome. (c) Leucosome microstructure with millimetric amphibole porphyroblast in a matrix made up of quartz, plagioclase and subordinate biotite. (d) Amphibole and oriented biotite in the mesosome sample.

(299-367 ppm). Th/U ratios are in the 0.2-0.5 range with lower Th/U ratio in the rims as compared to the cores.

Some selected analyses of amphibole and biotite of the two selected MES5 and LEU5 samples are reported in Table 2.

Amphibole from leucosome and mesosome is a potassian ferropargasite according to the classification of Leake et al. (1997) with X_{Mg}= Mg/(Mg + Fe^{2+}) ~0.4-0.5 and Ti in the 0.10-0.15 a.p.f.u. range. K_2O is between 1.7 and 1.9 wt.% and A(Na) +A(K) ranges from 0.55 to 0.80 a.p.f.u. The amphibole shows a slight compositional zoning with SiO_2- and MgO-rich, and K_2O-poor crystal rims. There is no significant difference in composition between leucosome and mesosome amphibole.

Biotite from LEU5 matrix has X_{Mg} ~0.44-0.49, whereas that from MES5 matrix has X_{Mg}~0.43-0.46. Biotite growing at the expense of amphibole and garnet has X_{Mg}=0.50 in both samples.

U-PB ZIRCON DATING

Results of U-Pb zircon geochronology are given in Table S1 of Supplementary information and shown in Figures 5, 6.

In MES5 forty-five zircon grains were analyzed and 15 analyses yielded concordant U-Pb dates that span in the range between 472 and 310 Ma (Figure 5a; Table S1). The oldest value (472 Ma) was obtained from the oscillatory zoning domain of a 100 μm-sized rounded crystal, whereas the three youngest ages (444, 433 and 310 Ma) were measured in correspondence of thin rims

Table 1. Y, Nb, Hf, Ta, Th, U and REE composition of zircon core and rim from leucosome sample LEU5 of amphibole-bearing migmatite.

	Zr_core	Zr_core	Zr_core	Zr_rim	Zr_rim	Zr_rim
Y	1385	1039	948	545	689	511
Nb	2.40	1.94	1.39	1.88	1.41	1.58
La	0.025	0.031	0.040	0.016	0.015	0.030
Ce	1.71	1.04	0.80	0.56	0.41	0.43
Pr	0.201	0.174	0.080	0.016	0.054	0.032
Nd	2.51	2.35	1.69	0.53	0.88	0.39
Sm	5.24	5.44	4.24	1.57	2.79	1.21
Eu	0.56	0.41	0.19	0.08	0.18	0.05
Gd	32.4	25.0	19.6	7.6	15.4	6.7
Tb	10.8	8.4	7.2	3.1	5.0	3.0
Dy	134	109	91	48	62	44
Ho	51	39	32	18	22	17
Tm	48	34	30	19	22	20
Yb	396	299	271	180	199	197
Lu	76	58	51	39	38	39
Hf	5229	3496	4867	4034	4432	4641
Ta	0.34	0.14	0.20	0.15	0.20	0.40
Th	89	62	54	27	36	22
U	167	121	110	76	83	83

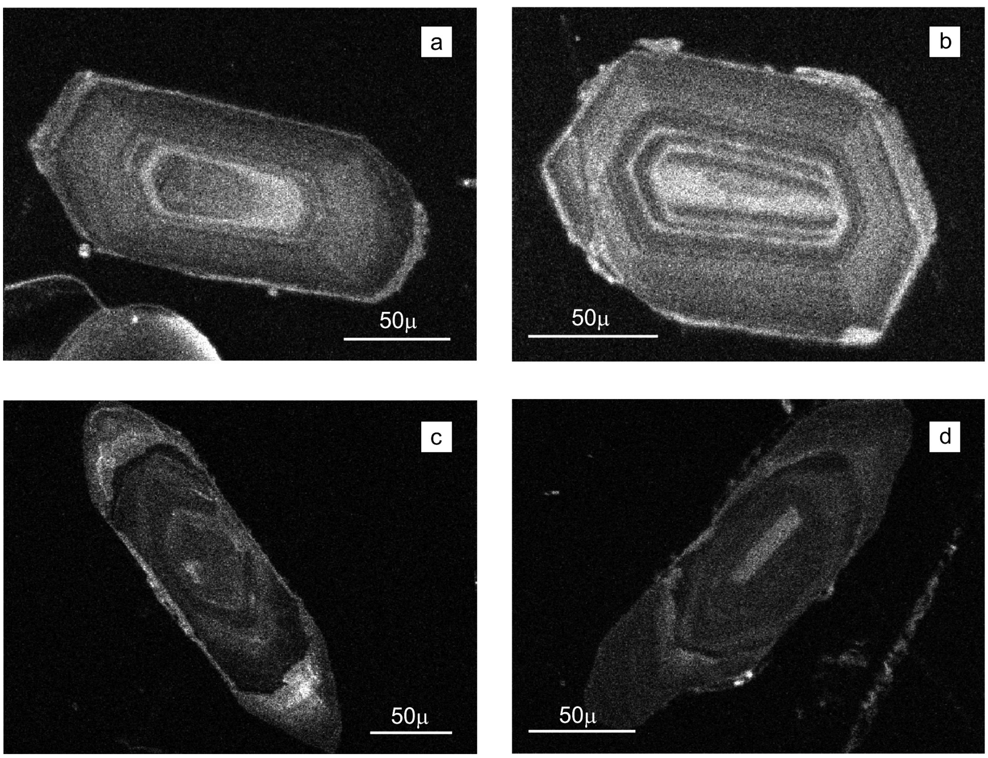

Figure 3. Selected CL images of zircons from the mesosome sample (a,b) and of the leucosome (c,d) of the amphibole-bearing migmatite of NE Sardinia. Grains (a), (b) show a concentric zoning of igneous origin; grains (c) and (d) show inherited core and overgrown rim.

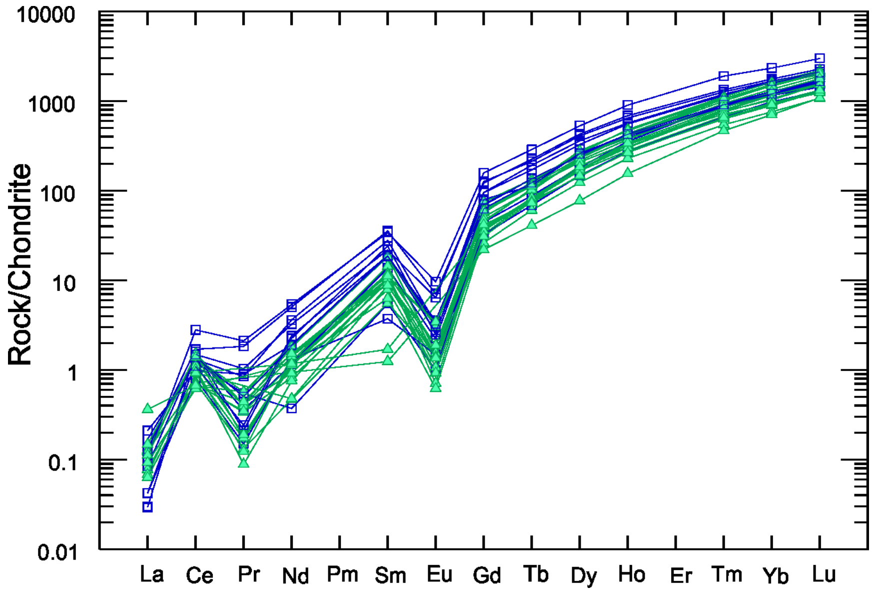

Figure 4. REE patterns normalized to chondrite values (McDonough and Sun, 1995) of zircon core (blue symbols) and rim (green) from leucosome sample. Additional analyses not reported in Table 2 are also shown.

Table 2. XRF bulk-rock chemistry of leucosome (LEU5) and mesosome (MES5) samples that were selected for geochronological investigation. Representative amphibole and biotite chemical composition from the amphibole-bearing migmatite samples is also shown.

	MES5	LEU5	Amp_{core}	Amp_{rim}	Bt
SiO_2	61.31	69.50	40.70	47.10	34.93
TiO_2	0.81	0.18	0.89	0.45	2.48
Al_2O_3	16.02	15.75	14.26	8.95	15.67
Cr_2O_3	-	-	0.03	0.00	0.02
Fe_2O_{3t}	6.93	2.71	-	-	-
FeO_t	-	-	17.51	16.90	20.85
MnO	0.12	0.02	0.27	0.32	0.20
MgO	3.38	1.45	8.28	10.90	10.78
CaO	4.32	4.77	11.70	11.10	-
Na_2O	2.53	3.73	1.10	1.02	0.12
K_2O	2.65	0.62	1.80	0.63	9.60
BaO	-	-	0.03	0.01	0.34
P_2O_5	0.17	0.04	-	-	-
LOI	1.72	0.84	-	-	-
Total	99.96	99.61	96.57	97.38	94.99

from elongated zircons that preserve a relict core. The remaining 11 out of 15 concordant U-Pb data cluster between 465 and 457 Ma (Darriwilian) with a weighted average of concordant data of 461.3±3.3 Ma (Figure 6a; MSWD=0.41 and probability of concordance=0.95).

In LEU5 sixty-four analyses were performed and 35 concordant U-Pb dates were obtained spanning between 485 and 290 Ma (Table S1). The two oldest ages (485 and 480 Ma) were obtained from the oscillatory zoning domain of two different ~100 µm-sized zircon crystals, whereas the two youngest ages of 297 and 290 Ma were measured in thin rims overgrowing a relict core. In the probability density plots for the U-Pb concordant ages shown in Figure 5b two main clusters can be recognized: an old zircon population (17 analyses mostly corresponding to zircon core domains or domains with oscillatory zoning) clustering at 460 Ma (Figure 6b, weighted average age of 462.5±2.4 Ma) and a younger population (10 analyses, mostly limited to rim domains) spanning in the 344-290 range with five samples being comprised in the 328-320 Ma range. The small cluster close to 325 Ma in Figure 5b resulted in a weighted average age of 324.2±4.0 Ma (MSWD 0.96; Figure 6c). Between the two clusters, six analyses yielded intermediate ages comprised between 447 and 352 Ma.

These results allow to identify the following two age clusters: i) Middle Ordovician (Darriwilian) protolith age at 462.5±2.4 Ma and ii) Middle Carboniferous (Serpukhovian) age of *ca*. 325 Ma, here interpreted as the age of migmatization. The youngest domains of zircons recovered from the studied samples are mostly related

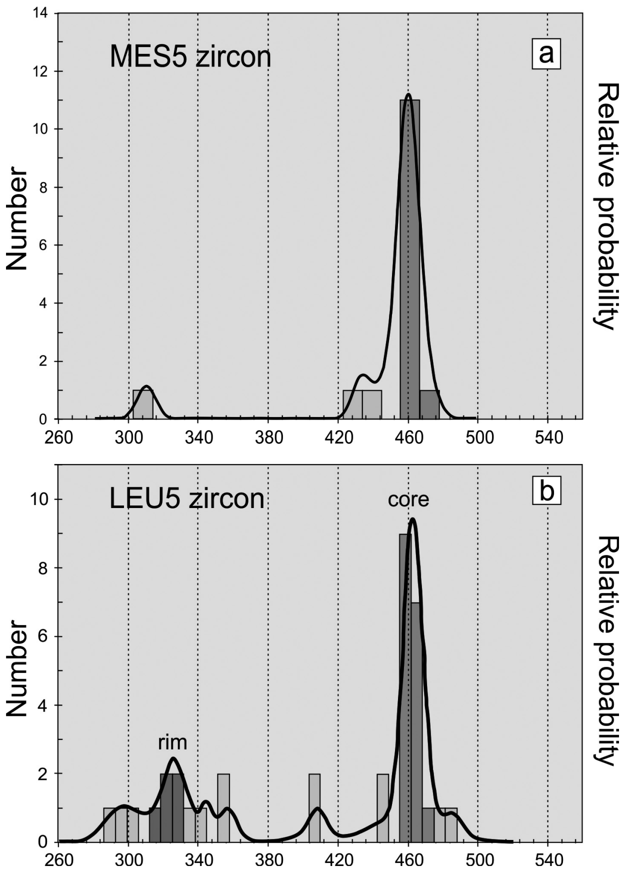

Figure 5. Probability density plots for the U-Pb concordant ages obtained for mesosome (a) and leucosome (b) of the amphibole-bearing migmatites. Dark grey values were used for the calculation shown in Figure 6.

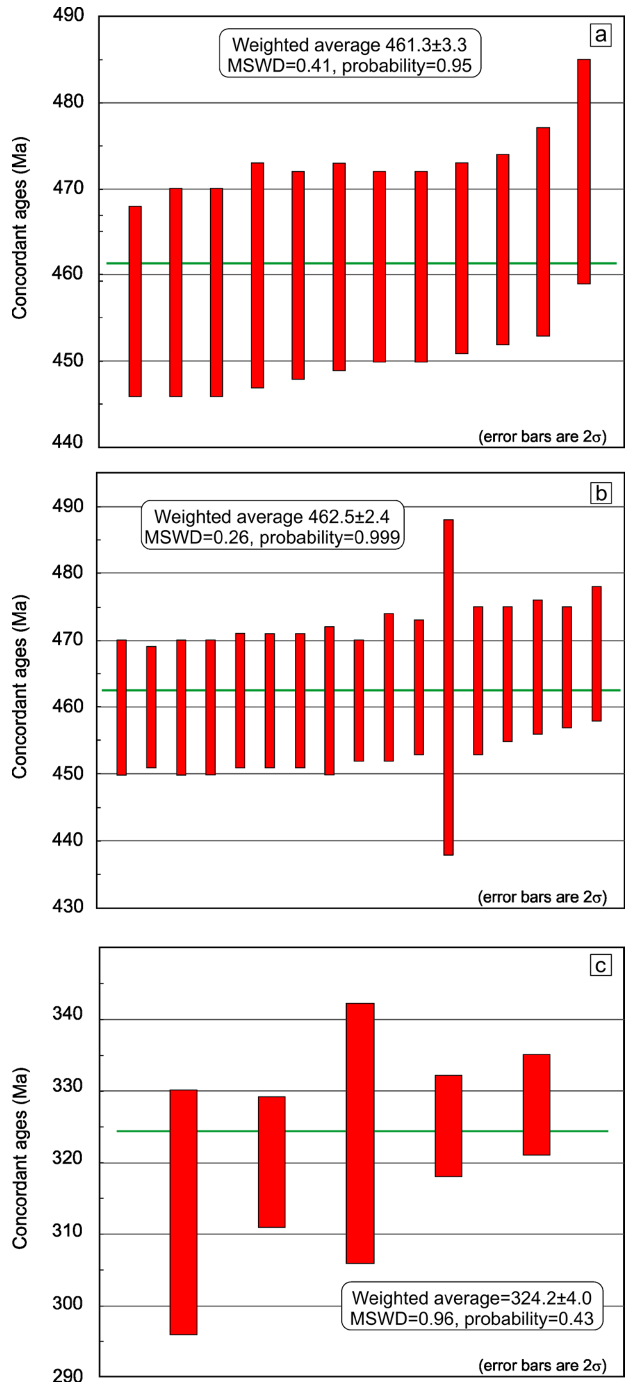

Figure 6. Weighted average $^{206}Pb/U^{238}$ age for: (a) MES5 zircons; (b) old zircon population (>380 Ma) in LEU5; (c) younger zircon population (<380 Ma) in LEU5.

to thin rim zircon domains overgrowing relict cores. The oldest ages of 485 to 472 Ma could represent inherited zircon grains or, according to the magmatic growth zoning observed in the zircon grain, the very beginning of igneous protolith crystallization. The ages ranging 460-328 Ma that are intermediate between the two main clusters in the leucosome could be eventually related to mixing of old zircon cores with young rims or to partial zircon resetting during metamorphism.

AR-AR GEOCHRONOLOGY ON AMPHIBOLE AND BIOTITE

Amphibole - The complete analytical dataset obtained from a 4.6 mg amphibole separate analysed with ^{40}Ar-^{39}Ar laser step-heating technique is reported in Table 3, whereas the diagram of age (in Ma) vs cumulative ^{39}Ar released (in %) is shown in Figure 7a. Seventeen consecutive steps from intermediate- to high-temperature region yielded an age profile characterized by a concordant segment representing ~75% of the ^{39}Ark released, yielding an error weighted mean age of 317.4±2 Ma (MSWD 1.54). We believe that this age is strictly related to the migmatite cooling at T <500-560 °C, roughly corresponding to the amphibole closure temperature in the ^{40}Ar-^{39}Ar isotope system (450-525 °C, Spear et al., 1993, pag. 719).

Biotite - The analytical data obtained from five biotite

Table 3. Results of laser step-heating $^{40}Ar/^{39}Ar$ dating for a 4.6mg amphibole separate and five biotite flakes from the amphibole-bearing migmatites of Punta Sirenella.

No.	$^{36}Ar(atm)$	±2σ	$^{37}Ar(Ca)$	±2σ	$^{38}Ar(Cl)$	±2σ	$^{39}Ar(K)$	±2σ	$^{40}Ar(Tot)$	±2σ	Age	±2σ	$^{40}Ar^*$	^{39}ArK	Ca/K	±2σ
Amphibole																
89A	4.77E-03	1.37E-04	1.32E-02	2.00E-03	4.33E-04	1.14E-04	4.11E-03	1.52E-04	1.68E+00	1.25E-03	581	77	16.0	0.1	6.1	1.1
89B	7.00E-04	7.22E-05	1.54E-02	1.94E-03	1.51E-04	7.69E-05	9.04E-03	1.57E-04	5.34E-01	1.34E-03	343	21	61.3	0.3	3.21	0.52
89C	1.93E-04	4.62E-05	1.61E-02	2.23E-03	1.66E-04	4.40E-05	1.45E-02	1.15E-04	4.95E-01	8.21E-04	291.3	8.7	88.5	0.4	2.10	0.36
89E	3.43E-04	4.97E-05	1.64E-01	9.29E-03	2.52E-03	1.04E-04	4.18E-02	2.44E-04	1.45E+00	1.59E-03	308.1	3.5	93.0	1.2	7.39	0.85
89F	3.14E-04	1.03E-04	1.46E+00	7.88E-02	2.93E-02	4.62E-04	3.11E-01	1.51E-03	1.03E+01	7.73E-03	314.7	1.7	99.1	8.8	8.9	1.0
89H	1.55E-04	1.68E-04	2.68E+00	1.45E-01	5.97E-02	8.02E-04	6.14E-01	2.76E-03	2.05E+01	1.70E-02	318.7	1.5	99.7	17.3	8.24	0.94
89I	4.78E-07	1.63E-04	2.49E+00	1.34E-01	5.84E-02	8.53E-04	6.04E-01	3.71E-03	2.01E+01	8.92E-02	317.5	2.3	100.0	17.1	7.76	0.88
89J	7.27E-05	1.76E-04	2.74E+00	1.48E-01	6.57E-02	9.85E-04	6.84E-01	3.27E-03	2.26E+01	2.21E-02	316.0	1.6	99.9	19.3	7.55	0.86
89L	7.93E-05	1.52E-04	2.00E+00	1.08E-01	4.87E-02	6.59E-04	5.05E-01	4.02E-03	1.68E+01	6.41E-02	317.5	2.7	99.8	14.3	7.46	0.85
89M	2.82E-05	9.29E-05	1.03E+00	5.61E-02	2.47E-02	3.60E-04	2.57E-01	1.13E-03	8.55E+00	9.06E-03	317.2	1.6	99.9	7.3	7.58	0.86
89N	2.13E-05	5.14E-05	3.39E-01	1.87E-02	7.33E-03	2.22E-04	8.02E-02	5.91E-04	2.61E+00	3.56E-03	311.3	2.7	99.7	2.3	7.98	0.91
89Q	2.01E-05	4.30E-05	3.23E-01	1.81E-02	7.01E-03	1.74E-04	7.56E-02	3.55E-04	2.56E+00	2.04E-03	322.1	2.0	99.7	2.1	8.05	0.92
89R	5.08E-06	6.34E-05	2.37E-01	1.33E-02	5.11E-03	1.61E-04	5.72E-02	3.72E-04	1.93E+00	1.15E-03	322.0	3.4	99.9	1.6	7.81	0.90
89S	1.35E-06	5.26E-05	2.07E-01	1.16E-02	4.75E-03	9.66E-05	5.03E-02	3.44E-04	1.68E+00	1.68E-03	318.7	3.4	99.9	1.4	7.74	0.89
89U	6.20E-07	3.88E-05	4.36E-01	2.40E-02	9.41E-03	2.56E-04	9.88E-02	4.47E-04	3.28E+00	2.42E-03	316.8	1.7	100.0	2.8	8.33	0.95
89V	7.22E-06	6.60E-05	5.67E-01	3.10E-02	1.05E-02	1.90E-04	1.12E-01	6.49E-04	3.72E+00	1.82E-03	317.4	2.3	99.9	3.2	9.6	1.1
89W	5.79E-05	4.16E-05	1.34E-01	7.71E-03	1.97E-03	8.85E-05	2.12E-02	2.24E-04	7.13E-01	1.45E-03	313.7	6.0	97.6	0.6	11.9	1.4
Biotite																
88B	3.71E-03	9.98E-05	2.02E-02	2.18E-03	1.65E-03	1.34E-04	7.36E-02	4.08E-04	1.49E+00	1.89E-03	54.6	4.1	26.27	2.8	0.52	0.08
88C	9.18E-04	6.32E-05	1.17E-04	1.64E-03	8.13E-04	8.96E-05	4.46E-02	3.18E-04	7.92E-01	8.65E-04	118.1	4.2	65.74	1.7	0.005	0.069
88E	1.12E-03	5.58E-05	4.96E-04	1.67E-03	2.73E-03	1.83E-04	1.82E-01	7.68E-04	4.85E+00	3.86E-03	242.6	1.3	93.16	6.8	0.005	0.017
88F	8.94E-04	7.48E-05	9.24E-04	1.81E-03	5.10E-03	3.61E-04	3.95E-01	1.71E-03	1.20E+01	1.07E-02	287.5	1.3	97.77	14.8	0.004	0.009
88G	5.46E-04	4.27E-05	1.34E-03	1.69E-03	4.11E-03	2.84E-04	3.18E-01	1.43E-03	9.96E+00	4.65E-03	296.2	1.3	98.35	11.9	0.008	0.010
88H	2.67E-04	5.19E-05	9.47E-04	1.75E-03	2.71E-03	1.84E-04	2.04E-01	9.24E-04	6.47E+00	7.07E-03	301.1	1.5	98.75	7.7	0.009	0.016
88I	2.94E-04	4.77E-05	8.37E-04	1.69E-03	3.20E-03	2.59E-04	2.49E-01	1.11E-03	7.94E+00	3.84E-03	302.6	1.3	98.87	9.4	0.006	0.013
88J	4.57E-04	3.11E-05	1.07E-04	1.81E-03	3.51E-03	2.43E-04	2.62E-01	1.12E-03	8.27E+00	5.65E-03	298.7	1.2	98.33	9.8	0.001	0.013
88K	2.91E-04	5.08E-05	4.74E-04	1.80E-03	1.73E-03	1.89E-04	1.35E-01	7.93E-04	4.24E+00	3.22E-03	296.8	1.9	97.94	5.1	0.007	0.025
88L	3.85E-04	2.59E-05	8.44E-04	1.79E-03	2.52E-03	2.15E-04	2.03E-01	1.10E-03	6.40E+00	3.80E-03	297.9	1.5	98.19	7.6	0.008	0.017
88M	4.59E-04	1.45E-04	7.96E-04	1.69E-03	2.31E-03	1.82E-04	1.79E-01	1.01E-03	5.54E+00	1.06E-02	291.1	2.7	97.52	6.7	0.008	0.018
88O	2.86E-04	6.49E-05	2.70E-04	1.70E-03	1.67E-03	1.45E-04	1.33E-01	7.25E-04	4.08E+00	3.21E-03	289.4	2.0	97.89	5.0	0.004	0.024
88P	1.66E-04	5.07E-05	6.68E-04	1.72E-03	1.11E-03	1.32E-04	9.06E-02	5.03E-04	2.83E+00	2.40E-03	295.4	2.1	98.24	3.4	0.014	0.036
88Q	1.93E-05	4.59E-05	3.34E-04	1.79E-03	2.01E-04	6.28E-05	2.22E-02	2.30E-04	6.96E-01	9.50E-04	299.2	6.1	99.15	0.8	0.03	0.15
88R	2.49E-04	4.50E-05	4.38E-05	1.85E-03	2.06E-03	1.50E-04	1.72E-01	9.30E-04	5.39E+00	3.86E-03	297.0	1.6	98.60	6.5	0.000	0.020

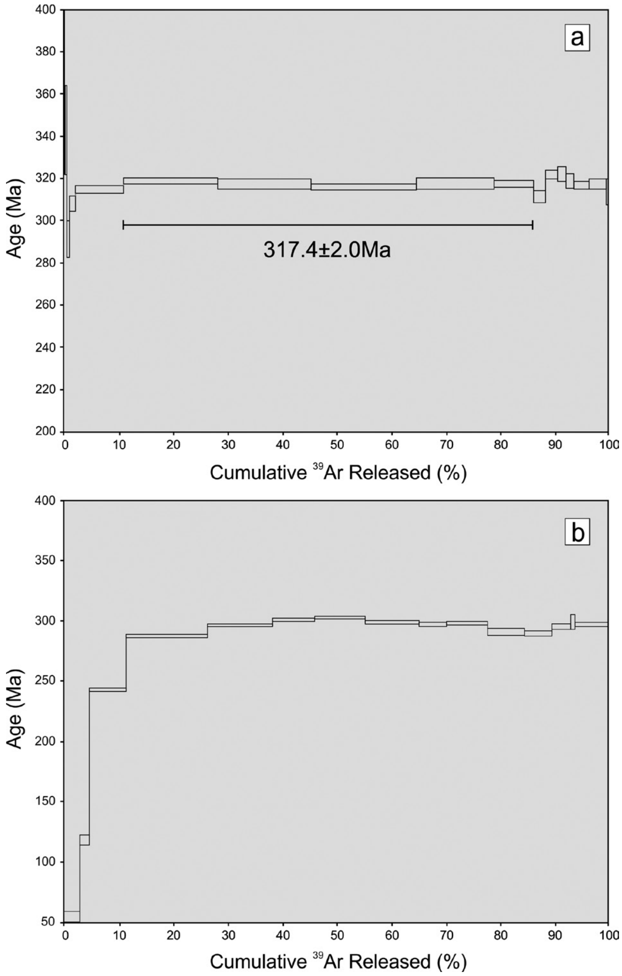

Figure 7. Age release spectrum of (a) amphibole concentrate and (b) biotite from the mesosome of the amphibole-bearing migmatite.

crystals that were analysed with ^{40}Ar-^{39}Ar laser step-heating technique are listed in Table 3, whereas the age (in Ma) vs cumulative ^{39}Ar released (in %) diagram is shown in Figure 7b. Fifteen steps yielded ages comprised between 54.6-302.6 Ma with 12 ages clustering in the 287.5-302.6 Ma age interval. The resulting age spectrum for biotite corresponds to a total gas age of ~283 Ma.

The biotite Ar-Ar age obtained in this work can be compared with those obtained from the same mineral by Di Vincenzo et al. (2004), who obtained a wide Ar-Ar biotite age interval from 240 Ma to 305-310 Ma for samples from the Migmatite Complex. Di Vincenzo et al. (2004) also observed that the biotite ages seem to be very sensitive to secondary alteration processes and that younger ages mainly come from areas where biotite is chloritized or characterized by pronounced parting along the basal cleavage. Based on these observations, we hypothesize that the biotite age spectrum (total gas age of 283 Ma), is hump-shaped most probably for the sporadic occurrence of minor interlayered chlorite.

DISCUSSION

Migmatite protolith age

In the amphibole-bearing migmatite from Punta Sirenella the obtained zircon ages allowed to identify two main age clusters at ~461 Ma and ~325 Ma, this latter mostly related to thin rim zircon domains.

The protolith age of 461 Ma obtained for the mesosome sample is coincident or very similar to those available from similar felsic rocks already studied in literature of the Sardinia-Corsica Variscan basement: Punta Sirenella migmatite: 461 Ma with whole rock Rb/Sr method, 452 Ma with zircon Kober technique, Cruciani et al. (2008); Golfo Aranci orthogneiss: 470-465 Ma, with in-situ U/Pb zircon geochronology, Giacomini et al. (2006); orthogneiss of NE Sardinia: 456±14 Ma, Helbing and Tiepolo (2005); Capo Ferro orthogneiss: 457±3 and 430±2 Ma U/Pb zircon geochronology, Padovano et al. (2014); Zicavo and Porto Vecchio orthogneisses, Corsica: 458±32 Ma and 465+19/-16 Ma, respectively , U-Pb method, Rossi et al. (2009); Lodè orthogneiss: 456±14 Ma, in situ U-Pb zircon age by Helbing and Tiepolo (2005). Comparable ages were also obtained from their mafic counterparts. For example, SHRIMP U-Pb dating of zircon of the Punta de li Tulchi retrogressed eclogites yielded a weighted mean protolith age of 453±14 Ma (Palmeri et al., 2004). A protolith age of 460±5 Ma was also obtained by Giacomini et al. (2005) from magmatic zircons in the Golfo Aranci eclogites, whereas an age of 457±2 Ma was obtained by Cortesogno et al. (2004) for a zircon population of eclogite from Migmatite Complex. Our new geochronological data on zircons, together with the above mentioned ones available in literature, indicate a widespread magmatic activity in the Middle Ordovician in the northern Gondwana margin.

Age of Variscan anatexis

The results obtained for the amphibole and biotite separates by the Ar/Ar method define the following ages: i) a Upper Carboniferous (Pennsylvanian) weighted mean age of 317.4±2 Ma (Bashkirian) for amphibole and (ii) a Lower Permian (Cisuralian) total gas age of 283 Ma (boundary Artinskian/Kungurian) for biotite. The age of layered migmatites in northern Sardinia (350-345 Ma, Ferrara et al., 1978; Giacomini et al., 2006) indicates that the beginning of anatexis under amphibolite facies conditions precedes the onset of emplacement of the granodioritic-monzogranite plutons (U2 magmatic sequence; 320-330 Ma; Rossi and Cocherie, 1991; Ferré and Leake, 2001) by at least 20 million years.

The younger zircon ages of the amphibole bearing migmatites obtained in this study cluster at *ca*. 325 Ma (Figures 5b, 6c) very similar to the U-Pb monazite age of 325±1.3 Ma for migmatitic orthogneiss of Capo Ferro area reported by Padovano et al. (2014) and interpreted by these authors as the age of migmatization, syntectonic to the shear deformation related to the East Variscan Shear Zone (Corsini and Roland, 2009; Elter et al., 2010; Padovano et al., 2012). A similar age (326±4 Ma) for migmatization was obtained by Giacomini et al. (2006) for diatexite from Golfo Aranci area (NE Sardinia). Palmeri et al. (2004) interpreted the zircon age of 327±7 Ma from the Punta de li Tulchi eclogite (NE Sardinia) as the Variscan overprint of eclogites.

The amphibole and biotite ages presented in this paper provide information on the moment of their isotopic closure as regards the Ar-Ar isotopic system and allow to better constrain the timing of anatexis and cooling of the amphibole-bearing migmatites from Punta Sirenella. For these rocks, Massonne et al. (2013) supposed a scenario where a igneous protolith of intermediate composition was metamorphosed at high pressure. At the final prograde stage of metamorphism, the amphibole-bearing migmatite attains P-T conditions of ~13 kbar and 700 °C. After this stage pressure decrease and slight cooling brought leucosomes to P-T conditions suitable for the growth and subsequent partial resorption of centimetric amphibole crystals. The resorption of amphibole crystals occurred likely at about 9 kbar and 680 °C, i.e. when the leucosome melt crossed the solidus P-T conditions (see Figure 10b in Massonne et al., 2013, p. 1502) just before the completion of the melt crystallization. The Bashkirian Ar-Ar age yielded by amphibole (317.4±2 Ma) is similar to the age of 320-300 Ma obtained by Di Vincenzo et al. (2004) for the syn-D_2 white mica in metasedimentary migmatite samples collected from the sillimanite+ K-feldspar zone in the Migmatite Complex of NE Sardinia. The oldest ages were found in the inner portions of the white mica flakes, the youngest in the rims. The 320-315 Ma time lapse, in its turn, is interpreted by Di Vincenzo et al. (2004) as the end of the chemical re-equilibration (including neo-crystallization) of white mica at upper-crustal levels during the D_2 phase. In this scenario, the similar ^{40}Ar-^{39}Ar age of 317.4±2 Ma we obtained on amphibole may be interpreted as the age of re-equilibration and cooling of this mineral. The value of 317.4±2 Ma closely recalls the U-Pb monazite age of 315±1.3 Ma obtained by Padovano et al. (2014) for the Capo Ferro orthogneiss, the 316 ± 5 Ma age yielded by the mylonites from Fautea-Solenzara (Corsica, Giacomini et al., 2008) and the 321.2+8.3 Ma age obtained by Oggiano et al. (2007) from the Cala Muro granite, Santa Maria Island. The first age, 315±1.3 Ma, was interpreted as dating the last thermal overprint of the orthogneiss, generated by the intrusion of the Capo Ferro syntectonic granites at 318 ± 3 Ma and 317±2 Ma (Padovano et al., 2014).

Considering that the 283 Ma biotite (Figure 7b) should be interpreted as a minimum Ar-Ar age due to the occurrence of interlayered chlorite, our data support the idea that migmatization started around 345 Ma and lasted for about 20 Ma, at least until *ca*. 325 Ma.

A useful framework for the new data discussed in the present paper is provided by the model proposed by Scodina et al. (2019, and references therein) who discussed the changing positions of amphibolites, eclogites and migmatites of NE Sardinia located in the northern Gondwana margin during the subduction of Gondwana below the peri-Gondwanan terranes previously accreted to Laurussia. The amphibolites, belonging to the lowermost hot part of the upper plate, initially located at 35 km depth (0.8-0.9 GPa) in the first phase of subduction (Upper Devonian), were brought during Tournaisian to a greater depth of 50-55 km (1.4 GPa). Eclogites in the cold subducting ocean crust at first arrived at a depth of about 70 km (2.0-2.2 GPa), before the detachment of the ocean crust, and then were broken, attached to the downgoing continental plate and exhumed in the subduction channel. Finally, after "a significant thrusting of Gondwana under Laurussia, around 345 Ma", the amphibolites, the migmatites, belonging to the uppermost part of the lower plate, and the slices of eclogites attached to the lower plate "were brought together and tectonically mixed within the exhumation channel during lower and middle Carboniferous times, probably starting in the Visean."

The striking coincidence between mineral ages from metamorphic rocks and emplacement ages of the Variscan granitoids has been explained in the past into the following two ways (Ferrara et al., 1978): (i) the heat supplied by the granitic intrusions could have caused a partial reopening of the mineral systems or, alternatively, (ii) the intrusions would have induced the uplift of the metamorphic sequences with the consequent temperature decrease and the closure of the mineral systems. The absence of thermometamorphic minerals (i.e. andalusite, cordierite) and textures in the migmatite, together with the occurrence of Permian volcanites lying directly on the metamorphic sequences of L-MGMC and granitoids in northern Sardinia (Ferrara et al., 1978) such as the Anglona region, seems to suggest that among the two aforementioned hypotheses the second one is the most probable. However, it cannot be excluded that migmatization and magmatism are both effects of a regional-scale thermal anomaly located in the deep portion of a thinned crust.

Sardinian migmatites in the framework of the Variscan belt

A careful examination of the geochronological data available in the literature (Table S2 of Supplementary information) reveals that 76% of ages are comprised in the 335-320 Ma interval, 12% in the 345-335 Ma and 12 % in the 320-310 Ma time interval. This clustering of 76 % of ages between 335 Ma and 320 Ma in a very restricted time lapse of only 15 million years reveals that actually the migmatization process took place simultaneously over an extremely wide area through the Variscan chain from Central Iberian Zone up to the Bohemian Massif, passing through Pyrenean region, South Armorican Massif, French Massif Central, Montagne Noire, Maures-Tanneron Massif, Corsica, Sardinia, Alpine External Massifs and Vosges (see references for each region in Table S2). Noteworthy are the unusual distances of 800 km between the Central Iberian Zone (Toledo) and the South Armorican Massif (Nantes) and of 1,200 km between the South Armorican Massif and the Bohemian Massif (Prague). The almost simultaneous migmatite production in only 15 million years (335-320 Ma) in several microplates with different tectono-metamorphic histories, from Central Iberian Zone to the Bohemian Massif in a 2,000 km long, 500-600 km large continental area arises the question to find a unique heat source active at a continental scale.

Two main hypotheses have been proposed in literature concerning the heat sources and the mechanisms through which migmatites and huge volumes of granitoid intrusions were generated within the Variscan Belt: 1) heat produced by radioactive elements, abundant in a thickened crust (Gerdes et al., 2000; Vanderhaeghe and Teyssier, 2001); 2) heat supplied by upwelling asthenospheric mantle undergoing decompression melting caused, during the late Variscan extensional tectonics, by lithospheric thinning, delamination of lithospheric mantle, slab breakoff and detachment or roll back of the Benioff plane (von Blankenburg and Davies, 1995; Anderson, 2005; Faure et al., 2009; Finger et al., 2009; Stampfli et al., 2013; Laurent et al., 2017). As regards the first hypothesis, Gerdes et al. (2000) for the South Bohemian Batholith and Vanderhaeghe and Teyssier (2001) for the Canadian Cordillera estimated that mainly the radiogenic heat produced by a thickened crust, after a few tens of million years, may cause a temperature increase able to generate huge volumes of granitic melts without a significant contribution of heat from the mantle. This model was proposed by Bea et al. (2003) and Pereira et al. (2008) in order to define the origin of the granitoid bodies emplaced in the Central Iberian Zone during the time interval 320-290 Ma, 30 million years after the beginning of anatexis at 352 Ma (Montero et al., 2004). Bea et al. (2003) and Pereira et al. (2008) disregard the possible role of a mantle source and ascribe the generation of the Variscan anatectic granitoids in the Central Iberian Zone to the radiogenic crustal heat source. Considering now the second hypothesis of an upwelling asthenosphere, two possible major heat sources may be hypothesized to account for the genesis of migmatites mainly in a short time frame of 15my over a distance of about 2,000 km: (i) subduction of a mid-ocean ridge or (ii) breakoff and detachment of a subducted oceanic slab (von Blankenburg and Davies, 1995) and delamination of the lithospheric mantle along the Moho discontinuity (Anderson, 2005; Finger et al., 2009). Both processes cause an extensive decompression melting in the lithospheric mantle. The first proposal of mid-ocean ridge subduction was put forward by Bussy et al. (2000). Afterwards, Stampfli et al. (2013), describing the evolution of the Paleotethys, state that "the mid-ocean ridge subduction took place between 340 and 320 Ma." The same authors, speaking about the complex history of the Paleotethys in the 350-310 Ma time lapse (their Figure 6 and p. 13), conclude that "these numerous and repeated lithospheric events where the asthenosphere/lithosphere boundary is rapidly changing could explain the large number of migmatite formation and granite intrusion at that time." According to von Raumer et al. (2014, Figure 3) southward dipping Rhenohercynian mid-ocean ridge and northward dipping Paleotethys mid-ocean ridge were subducted at 350-330 Ma underneath the collage of the Galatian terranes (Helvetic, Moldanubian, Saxothuringian blocks) and the Hanseatic terranes (Mid-German Rise), embryo of the future Variscan Belt. After the main collisional phase, the occurrence, beneath the Variscan Belt, of two buried mid-ocean ridges likely still active throughout the entire length of an evolving Variscan Belt could be a potential and reliable heat source able to trigger the almost simultaneous genesis of migmatites everywhere in the Variscan Europe.

As regards the second option, breakoff and detachment of a subducted slab and delamination of the lithospheric mantle, Kalt et al. (1999) hypothesize that downward detachment of thickened lithosphere in the mantle and upwelling asthenosphere provided heat for crustal melting and generation of migmatites in the Bohemian Massif.

Faure et al. (2009) attribute a Visean crustal melting event from the Armorican Massif to Vosges and the coeval magmatism in Massif Central and Vosges to the heat supplied by rising asthenosphere as a result of delamination of the lithospheric mantle along the Moho discontinuity.

Finally, according to Laurent et al. (2017) the Variscan magmatism active for 35-40 million years in the French Massif Central, "characterized by coeval melting of both crustal and mantle sources" reveals the existence of "a lithospheric-scale thermal anomaly", created by "a progressive southward delamination of the lithospheric mantle".

To the same trigger, "lithospheric mantle delamination", and to thermal softening of the thickened crust, causing gravitational collapse and extensional tectonics in the waning stages of the Variscan Orogeny, Rey et al. (1997) ascribe, among other consequences: 1) the production of large volumes of granitic magmas through "extensive melting and pervasive flow of the middle and lower crust"; 2) "widespread low-*P*-high-*T* metamorphic conditions"; 3) "mantle-derived mafic intrusion in the lower crust".

As regards Sardinia, Gaggero et al. (2017) state that a genetic correlation of the 332±12 Ma old Cobingius andesite from SE Sardinia with the 340 Ma old Mg-K suite of Corsica "cannot be excluded" and that the Mg-K suite is the "result of mantle melting and subsequent mixing with lower crustal material". Similarly, according to Paquette et al. (2003), the high K-Mg granitoids of Corsica, emplaced at 338±2 Ma, "display petrographic and geochemical hybrid characteristics…compatible with a significant involvement of…partial melts extracted from the shallow upper mantle. Furthermore Gaggero et al. (2017, Figure 3) reveal an almost continuous silicic magmatism, mainly consisting of rhyolitic ignimbrites, during a very long time lapse from the age of 321.2±8.3 Ma yielded by Cala Muro granite, Santa Maria island, ~40 km north of the Posada-Asinara Line (Oggiano et al., 2007) to the U-Pb zircon age of 275.6±3.4 Ma obtained by M. Maino, 2012 (personal communication to Edel et al., 2014) for the Gallura ignimbrite, Trinità d'Agultu, N Sardinia.

The whole scenario indicates the presence beneath Sardinia of a lithospheric scale heat source that could be represented by both buried mid-ocean ridges or upwelling molten asthenosphere for at least 45 Ma, resulting from the breakoff and downward detachment of a subducting slab or delamination of the lithospheric mantle. This scenario agrees with that proposed for the whole Variscan Belt by Rey et al. (1997) in their general study on the relationship between Scandinavian Caledonides and Variscan Belt. These authors recognize a time interval of 50 million years between 340 Ma and 290 Ma for the genesis and emplacement of huge granite volumes and identify the time lapse 330-310 Ma for the low-*P*-high-*T* metamorphism, two features that strongly characterize the Variscan Orogeny.

CONCLUSIONS

The U-Pb zircon and Ar-Ar amphibole and biotite geochronological data suggest the following scenario for the migmatite formation. The igneous protolith of the amphibole-bearing migmatite was emplaced at 461.3±3.3 Ma and subsequently underwent high-grade metamorphic conditions and partial melting during the late LP/HT post-collisional phase of the Variscan Orogeny. The zircon core domains, in mesosome and leucosome, preserve Darriwilian to Sandbian ages whereas the zircon rim domains of leucosome point to an age, here interpreted as indicating the final stage of partial melting, at ~325 Ma. The zircon U-Pb ages do not give any indication of the beginning of partial melting. The ^{40}Ar-^{39}Ar amphibole age of 317.4±2 Ma, corresponding to the age of re-equilibration and cooling of the amphibole, is related to the time when migmatites were below the P-T conditions of partial melting, i.e. in sub-solidus conditions. According to these observations, partial melting in the Variscan chain of Sardinia probably lasted from 344 Ma to *ca*. 320-330 Ma. A comparison with the ages yielded by migmatites along the whole Variscan Belt indicates that, like in Sardinia, partial melting began around 345 Ma and was ubiquitous and synchronous in the 335-320 Ma time interval from Central Iberia to the Bohemian Massif.

SUPPLEMENTARY INFORMATION

Table S1, S2 are available for downloading at the Journal site.

APPENDIX

Zircons from MES5 and LEU5 were separated by crushing, heavy liquids processing and hand picking. Selected zircon grains, free of fractures and inclusions, were mounted in epoxy resin, polished and characterized for their internal textures by CL imaging. Selected trace elements (Y, Nb, Hf, Ta) and REE abundances in zircons were acquired at Cagliari University by using a Quadrupole ICP-MS Perkin Elmer Elan DRC-e coupled with a 213 nm Nd:YAG laser probe by New Wave Research. Measurements were made with 46-50 mJ laser energy, spot sizes of 40-100 mm, a pulse energy of 0.2 mJ, 50-60 s ablation, 60 s background, and 30 s washout delay. Data reduction was made with Glitter using 29Si as internal standard in concentrations determined by electron microprobe. U-Pb geochronology was performed by LA-ICPMS at the CNR-Istituto di Geoscienze e Georisorse-UOS, Pavia by using a 193-nm ArF excimer laser microprobe (Geolas200Q-Microlas) coupled with a Thermo Finnigan Element I ICPMS. The analytical method is reported in Tiepolo (2003). Instrumental and laser-induced U/Pb fractionations were corrected using zircon GJ-1 (Jackson et al., 2004) whereas reference zircon 91500 (Wiedenbeck et al., 1995) and 02123 (Ketchum et al., 2001) were analyzed together with unknown samples for quality control at each analytical run. Spot size was 25 μm for leucosome and mesosome, but measurements with 10 μm spot size were also performed for leucosome zircons. All analytical runs were carried out with laser fluency set to 8.8 J/cm^2. Data reduction was carried out using the ''Glitter'' software package (van Achterbergh et al., 2001). Concordia ages were determined, and relative probability plots were constructed using the Isoplot/EX 3.0 software (Ludwig, 2000), with uncertainties given at 2σ level. Biotite and amphibole separation and Ar-Ar analyses were fulfilled at Istituto di Geoscienze e Georisorse, CNR Pisa. Biotite and amphibole were separated by conventional methods. Amphibole grains were leached at ambient temperature in ultrasonic bath for 10' in HNO_3 (1N) and 5' HF (7%). The separated grains were irradiated with a neutron flux for 60 hours in the central canal of the nuclear reactor TRIGA of L.E.N.A., at the University of Pavia. The neutron flux was measured with the "Fish Canyon Tuff Sanidine" international standard (age of 28.03 Ma, Jourdan and Renne, 2007). Both minerals were analyzed with step-heating technique by continuous defocused laser beam generated by a laser Nd-heating: YAG laser (maximum power: 18 W). More details on the ^{40}Ar-^{39}Ar methodology are reported in Di Vincenzo and Skála (2009) and Di Vincenzo et al. (2010). Table 3 shows the complete analytical data, corrected after irradiation decay, instrumental mass fractionation effects, isotopes produced from interference reactions during irradiation and blanks. Argon isotope concentrations are in V. All the errors are given at 2σ level. Ages were calculated using the constants recommended by I.U.G.S. (Steiger and Jäger, 1977). The error provided for total and weighted average ages relative to concordant tract does not include the uncertainties associated with the constants of the ^{40}K decay and age of the monitor.

ACKNOWLEDGEMENTS

The authors are grateful to Reviewers Giovanni Musumeci (Pisa University) and Vanni Tecchiato (Roma - La Sapienza) that improved the final version of the manuscript. F. Podda and D. Fancello (Cagliari University) are acknowledged for assistance during LA-ICPMS work. Gianfranco di Vincenzo (CNR, Pisa) is acknowledged for ^{40}Ar-^{39}Ar laser analyses on amphibole and biotite. Financial support was provided by Università di Cagliari FdS-RAS funding F72F16003080002, and RAS-Progetti di Ricerca di base orientata, L.R. 7/2007-annualità 2010 (M. Franceschelli).

REFERENCES

Aguilar C., Liesa M., Castiñeiras P., Navidad M., 2014. Late Variscan metamorphic and magmatic evolution in the eastern Pyrenees revealed by U-Pb age zircon dating. Journal of the Geological Society 171, 181-192.

Anderson D.L., 2005. Large igneous provinces, delamination, and fertile mantle. Elements 2, 271-275.

Barca S., Carmignani L., Eltrudis A., Franceschelli M., 1995. Origin and evolution of the Permian-Carboniferous basin of Mulargia Lake (South-Central Sardinia, Italy) related to the Late-Hercynian extensional tectonics. Comptes Rendus de l'Académie des Sciences Série 2. Sciences de la terre et des planètes 321(2), 171-178.

Bea F., Montero P., González-Lodeiro F., Talavera C., Molina J.F., Scarrow J.H., Whitehouse M.J., Zinger T.F., 2006. Zircon thermometry and U-Pb ion-microprobe dating of the gabbros and associated migmatites of the Variscan Toledo Anatectic Complex, Central Iberia. Journal of the Geological Society 163, 847-855.

Bea F., Montero P., Zinger T., 2003. The nature, origin, and thermal influence of the granite source layer of Central Iberia. The Journal of Geology 111, 579-595.

Bé Mézème E., Cocherie A., Faure M., Legendre O., Rossi P., 2006. Electron microprobe monazite geochronology: a tool for evaluating magmatic age domains. Examples from the Variscan French Massif Central. Lithos 87, 276-288.

Bé Mézème E., Faure M., Cocherie A., Chen Y., 2005. In situ chemical dating of tectonothermal events in the French Variscan Belt. Terra Nova 17, 420-426.

Bouilhol P., Leyreloup A.F., Delor L., Vauchez A., Monié P., 2006. Relationships between lower and upper crust tectonic during doming: the mylonitic southern edge of the Velay metamorphic core complex (Cévennes-French Massif Central). Geodinamica Acta 19(3-4), 137-153.

Bussy F., Hernandez J., von Raumer J., 2000. Bimodal magmatism as a consequence of the post-collisional readjustment of the thickened Variscan continental lithosphere (Aiguilles Rouges-Mont Blanc Massifs, Western Alps). Transactions of the Royal Society of Edinburgh: Earth Sciences 91 (1-2), 221-233.

Carmignani L., Oggiano G., Barca S., Conti P., Salvadori I., Eltrudis A., Funedda A., Pasci S., 2001. Geologia della Sardegna. Note illustrative della Carta Geologica della Sardegna a scala 1:200000. Memorie descrittive della Carta Geologica d'Italia 60, 283 pp.

Casini L., Cuccuru S., Maino M., Oggiano G., Puccini A., Rossi Ph., 2014. Structural map of Variscan northern Sardinia (Italy). Journal of Maps 11(1), 75-84.

Casini L., Cuccuru S., Maino M., Oggiano G., Tiepolo M., 2012. Emplacement of the Arzachena Pluton (Corsica-Sardinia Batholith) and the geodynamics of incoming Pangaea. Tectonophysics 544-545, 31-49.

Casini L., Cuccuru S., Puccini A., Oggiano G., Rossi Ph., 2015. Evolution of the Corsica-Sardinia Batholith and late-orogenic shearing of the Variscides. Tectonophysics 646, 65-78.

Castiñeiras P., Navidad M., Liesa M., Carreras J., Casas J.M., 2008. U-Pb zircon ages (SHRIMP) for Cadomian and Lower Ordovician magmatism in the Eastern Pyrenees: new insights in the pre-Variscan evolution of the northern Gondwana margin. Tectonophysics 461, 228-239.

Cocherie A., Baudin T., Autran A., Guerrot C., Fanning C.M., Laumonier B., 2005. U-Pb zircon (ID-TIMS and SHRIMP) evidence for the early Ordovician intrusion of metagranites in the late Proterozoic Canaveilles Group of the Pyrenees and the Montagne Noire (France). Bulletin de la Société Géologique de France 176, 269-282.

Columbu S., Cruciani G., Fancello D., Franceschelli M., Musumeci G., 2015. Petrophysical properties of a granite-protomylonite-ultramylonite sequence: insight from the Monte Grighini shear zone, central Sardinia, Italy. European Journal of Mineralogy 27, 471-486.

Connolly J.A.D., Memmi I., Trommsdorff V., Franceschelli M., Ricci C.A., 1994. Forward modeling of calc-silicate microinclusions and fluid evolution in a graphitic metapelites, northeast Sardinia. American Mineralogist 79, 960-972.

Corsini M. and Rolland Y., 2009. Late evolution of the southern European Variscan belt: exhumation of the lower crust in a context of oblique convergence. Comptes Rendus Geoscience 341, 214-223.

Cortesogno L., Gaggero L., Oggiano G., Paquette J.-L., 2004. Different tectono-thermal evolutionary paths in eclogitic rocks from the axial zone of the Variscan chain in Sardinia (Italy) compared with the Ligurian Alps. Ofioliti 29, 125-144.

Cruciani G., Dini A., Franceschelli M., Puxeddu M., Utzeri D., 2010. Metabasite from the Variscan belt in NE Sardinia, Italy: within-plate OIB-like melts with very high Sr and low Nd isotope ratios. European Journal of Mineralogy 22, 509-523.

Cruciani G., Fancello D., Franceschelli M., Scodina M., Spano M.E., 2014b. Geothermobarometry of Al-silicate-bearing migmatites from the Variscan chain of NE Sardinia, Italy: A P-T pseudosection approach. Periodico di Mineralogia 83, 19-40.

Cruciani G., Franceschelli M., Caredda A.M., Carcangiu G., 2001. Anatexis in the Hercynian basement of NE Sardinia, Italy: a case study of the migmatite of Porto Ottiolu. Mineralogy and Petrology 71, 195-223.

Cruciani G., Franceschelli M., Foley S.F., Jacob D.E., 2014a. Anatectic amphibole and restitic garnet in Variscan migmatite from NE Sardinia, Italy: insights into partial melting from mineral trace elements. European Journal of Mineralogy 26, 381-395.

Cruciani G., Franceschelli M., Groppo C., 2011. P-T evolution of eclogite-facies metabasite from NE Sardinia, Italy: insights into the prograde evolution of Variscan eclogites. Lithos 121, 135-150.

Cruciani G., Franceschelli M., Groppo C., Oggiano G., Spano M.E., 2015a. Re-equilibration history and P-T path of eclogites from Variscan Sardinia, Italy: a case study from the medium-grade metamorphic complex. International Journal of Earth Sciences 104, 797-814.

Cruciani G., Franceschelli M., Jung S., Puxeddu M., Utzeri D., 2008. Amphibole-bearing migmatites from the Variscan Belt of NE Sardinia, Italy: Partial melting of mid-Ordovician igneous sources. Lithos 105, 208-224.

Cruciani G., Franceschelli M., Massonne H.-J., Musumeci G., Spano M.E., 2016. Thermomechanical evolution of the high-grade core in the nappe zone of Variscan Sardinia, Italy: the role of shear deformation and granite emplacement. Journal of Metamorphic Geology 34,321-342.

Cruciani G., Montomoli C., Carosi R., Franceschelli M., Puxeddu M., 2015b. Continental collision from two perspectives: A review of Variscan metamorphism and deformation in northern Sardinia. Periodico di Mineralogia 84, 657-699.

Demoux A., Schärer U., Corsini M., 2008. Variscan evolution of the Tanneron Massif, SE France, examined through U-Pb monazite ages. Journal of the Geological Society 165(2), 467-478.

Di Vincenzo G., Bracciali L., Del Carlo P., Panter K., Rocchi S., 2010. ^{40}Ar-^{39}Ar dating of volcanogenic products from the AND-2A core (ANDRILL Southern McMurdo Sound Project, Antarctica): correlations with the Erebus Volcanic Province and implications for the age model of the core. Bulletin of Volcanology 72, 487-505.

Di Vincenzo G., Carosi R., Palmeri R., 2004. The relationship between tectono-metamorphic evolution and argon isotope records in white mica: constraints from in situ ^{40}Ar-^{39}Ar laser analysis of the Variscan basement of Sardinia. Journal of Petrology 45, 1013-1043.

Di Vincenzo G., Skála R., 2009. ^{40}Ar-^{39}Ar laser dating of tektites from the Cheb Basin (Czech Republic): evidence for coevality with moldavites and influence of the dating standard on the age of the Ries impact. Geochimica et Cosmochimica Acta 73, 493-513.

Edel J.B., Casini L., Oggiano G., Rossi P., Schulmann K., 2014. Early Permian 90° clockwise rotation of the Maures-Esterel-Corsica-Sardinia block confirmed by new paleomagnetic data and followed by a Triassic 60° clockwise rotation. Geological Society of London Special Publication 405, 333-361.

Elter F.M., Padovano M., Kraus R.K., 2010. The Variscan HT metamorphic rocks emplacement linked to the interaction between Gondwana and Laurussia plates: structural constraints in NE Sardinia (Italy). Terra Nova 22, 369-377.

Fancello D., Cruciani G., Franceschelli M., Massonne H.-J., 2018. Trondhjemitic leucosomes in paragneisses from NE Sardinia: Geochemistry and P-T conditions of melting and crystallization. Lithos 304-307, 501-517.

Faure M., Bé Mézème E., Cocherie A., Melleton J., Rossi P., 2009. The South Millevaches Middle Carboniferous crustal melting and its place in the French Variscan Belt. Bulletin de la Société Géologique de France 180, 473-481.

Faure M., Cocherie A., Bé Mézème E., Charles N., Rossi Ph., 2010. Middle Carboniferous crustal melting in the Variscan Belt: New insights from U-Th-Pb_{tot}. monazite and U-Pb zircon ages of the Montagne Noire Axial Zone (southern French Massif Central). Gondwana Research 18, 653-673.

Ferrara G., Ricci C.A., Rita F., 1978. Isotopic ages and tectonometamorphic history of the metamorphic basement of northeastern Sardinia. Contributions to Mineralogy and Petrology 68, 99-106.

Ferré E.C. and Leake B.E., 2001. Geodynamic significance of early orogenic high-K crustal and mantle melts: Example of the Corsica Batholith. Lithos, 59(1-2),47-67.

Finger F., Gerdes A., Miloš R., Riegler G., 2009. The Saxo-Danubian Granite Belt: magmatic response to post-collisional delamination of mantle lithosphere below the south-western sector of the Bohemian Massif (Variscan Orogen). Geologica Carpathica, 60(3), 205-212.

Franceschelli M., Battaglia S., Cruciani G., Pasci S., Puxeddu M., 2017. Very low-temperature metamorphism in Ordovician metasedimentary rocks above and below the Sardic unconformity, SW Sardinia, Italy. International Journal of Earth Sciences 106, 531-548.

Franceschelli M., Memmi I., Ricci C.A., 1982. Ca distribution between garnet and plagioclase in pelitic and psammitic schists from the metamorphic basement of north eastern Sardinia. Contributions to Mineralogy and Petrology 80, 225-295.

Franceschelli M., Pannuti F., Puxeddu M., 1990. Texture development and PT time path of psammitic schist from the Hercynian chain of NW Sardinia (Italy). European Journal of Mineralogy 2, 385-398.

Franceschelli M., Puxeddu M., Cruciani G., 2005b. Variscan metamorphism in Sardinia, Italy: review and discussion. Journal of the Virtual Explorer, vol. 19.

Franceschelli M., Puxeddu M., Cruciani G., Dini A., Loi M., 2005a. Layered amphibolite sequence in NE Sardinia, Italy: remnant of a pre-Variscan mafic silicic layered intrusion? Contributions to Mineralogy and Petrology 149, 164-180.

Friedl G., 1997. U/Pb Datierungen an Zirconen und Monaziten aus Gesteinen vom österreichischen Anteil der Böhmischen Masse. PhD Thesis, University of Salzburg, Austria, 242 pp.

Gaggero L., Gretter N., Langone A., Ronchi A., 2017. U-Pb geochronology and geochemistry of late Palaeozoic volcanism in Sardinia (southern Variscides). Geoscience Frontiers 8(6), 1263-1284.

Gaggero L., Oggiano G., Funedda A., Buzzi L., 2012. Rifting and arc-related early Paleozoic volcanism along the north Gondwana margin: geochemical and geological evidence from Sardinia (Italy). The Journal of Geology 120, 273-292.

Gerdes A., Wörner G., Henk A., 2000. Post-collisional granite generation and HT-LP metamorphism by radiogenic heating: the Variscan South Bohemian Batholith. Journal of the Geological Society of London 157, 577-587.

Giacomini F., Bomparola R.M., Ghezzo C., 2005. Petrology and geochronology of metabasites with eclogite facies relics from NE Sardinia: constraints for the Palaeozoic evolution of Southern Europe. Lithos 82, 221-248.

Giacomini F., Bomparola R.M., Ghezzo C., Guldbransen H., 2006. The geodynamic evolution of Southern European Variscides: constraint from the U/Pb geochronology and geochemistry of the lower Paleozoic magmatic-sedimentary sequences of Sardinia (Italy). Contributions to Mineralogy and Petrology 152, 19-42.

Giacomini F., Dallai L., Carminati E., Tiepolo M., Ghezzo C., 2008. Exhumation of a Variscan orogenic complex: Insights into the composite granulitic-amphibolitic metamorphic basement of southeast Corsica (France). Journal of Metamorphic Geology 26, 403-436.

Helbing H. and Tiepolo M., 2005. Age determination of Ordovician magmatism in NE Sardinia and its bearing on Variscan basement evolution. Journal of the Geological Society 162, 689-700.

Jackson S.E., Pearson N.J., Griffin W.L., Belousova E.A., 2004. The application of laser ablation-inductively coupled plasma-mass spectrometry to in situ U-Pb zircon geochronology. Chemical Geology 211, 47-69.

Jourdan F. and Renne P.R., 2007. Age calibration of the Fish Canyon sanidine $^{40}Ar/^{39}Ar$ dating standard using primary K-Ar standards. Geochimica et Cosmochimica Acta 71, 387-402.

Kalt A., Berger A., Blümel P., 1999. Metamorphic evolution of cordierite-bearing migmatites from the Bayerische Wald (Variscan Belt, Germany). Journal of Petrology 40 (4), 601-627.

Kalt A., Corfu F., Wijbrans J.P., 2000. Time calibration of a P-T path from a Variscan high-temperature low pressure complex (Bayerische Wald, Germany) and the detection of inherited monazite. Contributions to Mineralogy and Petrology 138, 143-163.

Ketchum J.W.F., Jackson S.E., Culshaw N.G., Barr S.M., 2001. Depositional and tectonic setting of the Paleoproterozoic Lower Aillik Group, Makkovik Province, Canada: evolution of a passive margin-foredeep sequence based on petrochemistry and U-Pb (TIMS and LAM-ICP-MS) geochronology. Precambrian Research 105, 331-356.

Kratinová Z., Schulmann K., Edel J.B., Ježek J., Schaltegger U., 2007. Model of successive granite sheet emplacement in transtensional setting: Integrated microstructural and anisotropy of magnetite susceptibility study. Tectonics 26, TC6003.

Laurent O., Couzinié S., Zeh A., Vanderhaeghe O., Moyen J-F., Villaros A., Gardien V., Chelle-Michou C., 2017. Protracted, coeval crust and mantle melting during Variscan late-orogenic evolution: U-Pb dating in the eastern French Massif Central. International Journal of Earth Sciences 106(2), 421-451.

Leake B.E., Woolley A.R., Arps C.E.S., Birch W.D., Gilbert M.C., Grice J.D., Hawthorne F.C., Kato A., Kisch H.J., Krivivichev V.G., Linthout K., Laird J., Mandarino J.A., Maresch W.V., Nickel E.H., Rock N.M.S., Schumacher J.C., Smith D.C., Stephenson N.C.N., Ungaretti L., Whittaker E., Youzhi G., 1997. Nomenclature of amphiboles: report of the subcommittee on amphiboles of the International Mineralogical Association, commission on new minerals and mineral names. The Canadian Mineralogist 35, 219-246.

Li X.H., Faure M., Lin W., 2014. From crustal anatexis to mantle melting in the Variscan orogen of Corsica (France): SIMS U-Pb zircon age constraints. Tectonophysics 634, 19-30.

Ludwig K.R., 2000. Isoplot: a geochronological toolkit for

Microsoft Excel. Berkeley Geochronology Center. Berkeley, Special Publication 1a, 1-53.

Marcou E., Cocherie A., Ruffet G., Darboux J.-R., Guerrot C., 2009. Géochronologie revisitée du dôme du Léon (Massif armoricain, France). Géologie de la France 1, 19-40.

Massonne H.-J., Cruciani G., Franceschelli M., 2013. Geothermobarometry on anatectic melts - A high-pressure Variscan migmatite from northeast Sardinia. International Geology Review 55, 1490-1505.

Massonne H.-J., Cruciani G., Franceschelli M., Musumeci G., 2018. Anticlockwise pressure-temperature paths record Variscan upper-plate exhumation: example from micaschists of the Porto Vecchio region, Corsica. Journal of Metamorphic Geology 36, 55-77.

McDonough W.F. and Sun S.S., 1995. The composition of the Earth. Chemical Geology 120, 223-253.

Mezger J.E. and Gerdes A., 2016. Early Variscan (Visean) granites in the core of central Pyrenean gneiss domes: implications from laser ablation U-Pb and Th-Pb studies. Gondwana Research 29, 181-198.

Montero P., Bea F., Zinger T. F., Scarrow J.H., Molina J.F., Whitehouse M., 2004. 55 million years of continuous anataxis in Central Iberia: single-zircon dating of the Peña Negra Complex. Journal of the Geological Society 161, 255-263.

Mougeot R., Respaut J.P., Ledru P., Marignac C., 1997. U-Pb geochronology on accessory minerals of the Velay anatectic Dome (French Massif Central). European Journal of Mineralogy 9, 141-156.

Moussavou M., 1998. Contribution à l'histoire thermo-tectonique varisque du Massif des Maures par la typologie du zircon et la géochronologie U/Pb sur minéraux accessoires. PhD Thesis, University of Montpellier 2, France, 187 pp.

Musumeci G., Spano M.E., Cherchi G.P., Franceschelli M., Pertusati P.C., Cruciani G., 2015. Geological map of the Monte Grighini Variscan Complex (Sardinia, Italy). Journal of Maps 11(2), 287-298.

Oggiano G., Casini L., Rossi P., Mameli P., 2007. Long lived dextral strike-slip tectonics in the southern Variscan Belt: evidences from two synkynematic intrusions of North Sardinia (Italy). Géologie de la France 2, 142.

Oggiano G., Gaggero L., Funedda A., Buzzi L., Tiepolo M., 2010. Multiple early Palaeozoic volcanic events at the northern Gondwana margin: U-Pb age evidence from the Southern Variscan branch (Sardinia, Italy). Gondwana Research 17, 44-58.

Oliot E., Melleton J., Schneider J., Corsini M., Gardien V., Rolland Y., 2015. Variscan crustal thickening in the Maures-Tanneron massif (South Variscan belt, France): new in situ monazite U-Th-Pb chemical dating of high-grade rocks. Bulletin de la Société Géologique de France 186, 145-169.

Padovano M., Dörr W., Elter F.M., Gerdes A., 2014. The East Variscan Shear Zone: Geochronological constraints from the Capo Ferro area (NE Sardinia, Italy). Lithos 196-197, 27-41.

Padovano M., Elter F.M., Pandeli E., Franceschelli M., 2012. The East Variscan Shear Zone: new insights into its role in the Late Carboniferous collision in southern Europe. International Geology Review 54, 957-970.

Palmeri R., Fanning M., Franceschelli M., Memmi I., Ricci C.A., 2004. SHRIMP dating of zircons in eclogite from the Variscan basement in north-eastern Sardinia (Italy). Neues Jahrbuch für Mineralogie Monatshefte 2004, 275-288.

Paquette J.-L., Ménot R.-P., Pin C., Orsini J.-B., 2003. Episodic and short-lived granitic pulses in a post-collisional setting: evidence from precise U-Pb zircon dating through a crustal cross-section in Corsica. Chemical Geology 198, 1-20.

Pereira D., Rodriguez Alonso M.D., Salman K., 2008. Evidence of protolith contamination in the generation of an anatectic complex: Peña Negra, Central Spain. The Open Mineralogy Journal 2, 6-16.

Poller U. and Todt W., 2000. U-Pb single zircon data of granitoids from the High Tatra Mountains (Slovakia): implications for the geodynamic evolution. Earth and Environmental Science Transactions of the Royal Society of Edinburgh 91(1-2), 235-243.

Rey P., Burg J.P., Casey M., 1997. The Scandinavian Caledonides and their relationship to the Variscan belt. In Burg J. P.& Ford M. (eds), 1997 *Orogeny Through Time,* geological Society Special Publication No. 121, pp 179-200.

Rossi, P. and Cocherie, A., 1991. Genesis of a Variscan batholith: Field, petrological and mineralogical evidence from the Corsica-Sardinia batholith. Tectonophysics 195(2-4), 319-346.

Rossi P., Oggiano G., Cocherie A., 2009. A restored section of the "southern Variscan realm" across the Corsica-Sardinia microcontinent. Comptes Rendus Geoscience 341, 224-238.

Rubatto D., Ferrando S., Compagnoni R., Lombardo B., 2010. Carboniferous high-pressure metamorphism of Ordovician protoliths in the Argentera Massif (Italy), Southern European Variscan belt. Lithos 116(1-2), 65-76.

Rubatto D., Schaltegger U., Lombardo B., Compagnoni R., 2001. Complex Paleozoic magmatic and metamorphic evolution in the Argentera Massif (Western Alps) resolved with U-Pb dating. Schweizerische Mineralogische und Petrographische Mitteilungen 81(2), 213-228.

Schaltegger U., Fanning C.M., Günther D., Maurin J.C., Schulmann K., Gebauer D., 1999. Growth, annealing and recrystallization of zircon and preservation of monazite in high grade metamorphism: conventional and in-situ U-Pb isotope, cathodoluminescence and microchemical evidence. Contributions to Mineralogy and Petrology 134, 186-201.

Schulmann K., Schaltegger U., Ježek J., Thompson A.B., Edel J.B., 2002. Rapid burial and exhumation during orogeny: Thickening and synconvergent exhumation of thermally weakened and thinned crust (Variscan orogeny in Western Europe). American Journal of Science 302, 856-879.

Scodina M., Cruciani G., Franceschelli M., Massonne H.-J.,

2019. Anticlockwise P-T evolution of amphibolites from NE Sardinia, Italy: geodynamic implications for the tectonic evolution of the Variscan Corsica-Sardinia block. Lithos 324-325, 763-775.

Spear F.S, 1993. Metamorphic phase equilibria and pressure-temperature-time paths. Mineralogical Society of America, 799 pp.

Stampfli G.M., Hochard C., Vérard C., Wilhem C., von Raumer J., 2013. The formation of Pangea. Tectonophysics 593, 1-19.

Steiger R.H. and Jäger E., 1977. Subcommission on geochronology: convention on the use of decay constants in geo- and cosmochronology. Earth and Planetary Science Letters 36, 359-362.

Tiepolo M., 2003. In situ Pb geochronology of zircon with laser ablation inductively coupled plasma-sector field mass spectrometry. Chemical Geology 199, 159-177.

Tropper P., Deibl I., Finger F., Kaindl R., 2006. P-T-t evolution of spinel-cordierite-garnet gneisses from the Sauwald Zone (Southern Bohemian Massif, Upper Austria): is there evidence for two independent late-Variscan low-P/high-T events in the Moldanubian Unit? International Journal of Earth Sciences 95 (6), 1019-1037.

Turrillot P., Augier R., Faure M., 2009. The top-to-the-East Sarzeau Shear Zone and its place in the syn-orogenic extensional tectonics of Southern Armorica. Bulletin de la Société Géologique de France 180, 247-261.

van Achterbergh E., Ryan C.G., Jackson S.E., Griffin W., 2001. Data reduction software for LA-ICP-MS. In: Laser Ablation-ICPMS in the Earth Science, Sylvester P (ed) Mineralogical Association of Canada: St. John's Newfoundland 29, 239-243.

Vanderhaeghe O. and Teyssier C., 2001. Crustal-scale rheological transitions during late-orogenic collapse. Tectonophysics 335, 211-228.

von Blankenburg F. and Davies J.H., 1995. A model for syncollisional magmatism and tectonics in the Alps. Tectonics 14 (1), 120-131

von Raumer J., Finger F., Veselá P., Stampfli G.M., 2014. Durbachites-Vaugnerites - a geodynamic marker in the central European Variscan orogen. Terra Nova 26, 85-95.

Wiedenbeck M., Alle P., Corfu F., Griffin W.L., Meier M., Ober F., von Quadt A., Roddick J.C., Spiegel J., 1995. Three natural zircon standards for U-Th-Pb, Lu-Hf, trace element and REE analysis. Geostandard Newsletter 19, 1-23.